J Med Syst (2018) 42: 2
https://doi.org/10.1007/s10916-017-0845-x

IMAGE & SIGNAL PROCESSING

Alcoholism Detection by Data Augmentation and Convolutional Neural Network with Stochastic Pooling

Shui-Hua Wang[1,2] · **Yi-Ding Lv**[3] · **Yuxiu Sui**[3] · **Shuai Liu**[4] · **Su-Jing Wang**[5] · **Yu-Dong Zhang**[1]

Received: 30 August 2017 / Accepted: 23 October 2017 / Published online: 17 November 2017

Abstract Alcohol use disorder (AUD) is an important brain disease. It alters the brain structure. Recently, scholars tend to use computer vision based techniques to detect AUD. We collected 235 subjects, 114 alcoholic and 121 non-alcoholic. Among the 235 image, 100 images were used as training set, and data augmentation method was used. The rest 135 images were used as test set. Further, we chose the latest powerful technique—convolutional neural network (CNN) based on convolutional layer, rectified linear unit layer, pooling layer, fully connected layer, and softmax layer. We also compared three different pooling techniques: max pooling, average pooling, and stochastic pooling. The results showed that our method achieved a sensitivity of 96.88%, a specificity of 97.18%, and an accuracy of 97.04%. Our method was better than three state-of-the-art approaches. Besides, stochastic pooling performed better than other max pooling and average pooling. We validated CNN with five convolution layers and two fully connected layers performed the best. The GPU yielded a 149× acceleration in training and a 166× acceleration in test, compared to CPU.

Keywords Alcohol use disorder · Data augmentation · Convolutional neural network · Max pooling · Average pooling · Stochastic pooling · Graphical processing unit

This article is part of the Topical Collection on *Image & Signal Processing*

✉ Shuai Liu
cs_liushuai@imu.edu.cn

✉ Su-Jing Wang
wangsujing@psych.ac.cn

✉ Yu-Dong Zhang
yudongzhang@ieee.org

[1] Department of Informatics, University of Leicester, Leicester LE1 7RH, UK

[2] School of Electronic Science and Engineering, Nanjing University, Nanjing, Jiangsu 210046, China

[3] Department of Psychiatry, Nanjing Brain Hospital, Nanjing Medical University, Nanjing, Jiangsu 210029, China

[4] College of Computer Science, Inner Mongolia University, Hohhot 010012, China

[5] Key Laboratory of Behavior Sciences, Institute of Psychology, Chinese Academy of Sciences, Beijing 100101, China

Introduction

Alcohol use disorder (shorted as AUD) affected 208 million people worldwide in 2010. It can cause severe adverse effects to the brain, liver, heart, and pancreas [1]. The long-term misuse can lead to increased tolerance to alcohol, making it difficult to control the consumption. The short-term misuse can lead to "blood alcohol concentration (BAC)". A BAC from 0.35% to 0.80% can cause fatal respiratory depression and life-threating alcohol poisoning [2].

This paper studies the effect of long-term misuse on the brain. As is known, patients with long-term AUD have smaller volumes of white matter and gray matter [3] than age-matched controls. Besides, alcohol causes adverse effect on the prefrontal cortex [4] and cerebellum [5]. Hence, we can create a healthcare system that monitors the patient brain via magnetic resonance imaging (MRI), and gives suggestions whether the patient is an alcoholic or healthy. MRI can give better resolution on brain soft tissues than

Table 1 Demographic characteristics

	Alcoholic		Nonalcoholic	
	Women (n = 56)	Men (n = 58)	Women (n = 62)	Men (n = 59)
Age (y)	59.0+ 8.0	56.5+ 8.9	56.9+ 8.4	55.3+ 7.9
Education (y)	9.9+ 1.9	9.3+ 1.6	9.6+ 2.4	9.3+ 2.5
DOHD (y)	13.2+ 3.5	19.6+ 5.4	0.0 ± 0.0	0.0 ± 0.0
DDE (gram/d)	197.6 + 62.1	300.7 + 92.1	6.8+ 4.7	4.9+ 3.8
LOS (y)	9.8+ 5.1	6.7+ 3.4	–	–
AUDIT	25.1+ 4.2	25.4+ 4.9	1.5+ 2.0	1.6+ 2.2

other imaging devices. CT is not used, since the X-ray in CT may do harm to the subjects.

In the last decade, scholars tend to detect alcoholism use brain imaging technique [6–8]. The radiologists may miss the slight shrinkage of AUD brains; therefore, a massive of computer vision based techniques have been proposed. Fisher et al. [9] offered a comprehensive review of medical robotic systems for use. Nayak et al. [10] presented a brain image classification algorithm based on random forest. Alweshah, Abdullah [11] hybridized firefly algorithm (FA) and probabilistic neural network (PNN). Lv, Hou [12] proposed an improved particle swarm optimization (IPSO) to detect alcoholism in MRI scanning. Monnig [13] suggested to detect white matter atrophy in neuroimaging of AUD. Yang [14] combined Hu moment invariant (HMI) and support vector machine (SVM). Do et al. [15] researched patients with multiple hypervascular hyperplastic liver nodules, and without alcohol abuse history. Matsui et al. [16] investigated neuroimaging to alcohol-related dementia in clinical applications. Zahr et al. [17] surveyed pathological and clinical features over brain damages due to alcohol.

Recently, convolutional neural network (CNN) has won remarkable achievement, such as AlphaGo [18] with Sedol Lee. This study aims to apply CNN to the alcoholism identification based on brain magnetic resonance images. In addition, we compared three pooling techniques: max pooling, average pooling, and stochastic pooling.

The structure of this paper is organized as follows: First section provides the subjects, scan protocol, slice selection and data augmentation method. Third section offers the fundamentals of convolutional neural network, particularly on the pooling layer. Fourth section gives the experiments and results. We showed the data augmentation result, CNN structure and training, the performance over test set, comparison to state-of-the-art methods, and comparison of different pooling methods. We also validated the optimal CNN structure, and gave the computation time by CPU and GPU, respectively. Finally, fifth section offers concluding remarks.

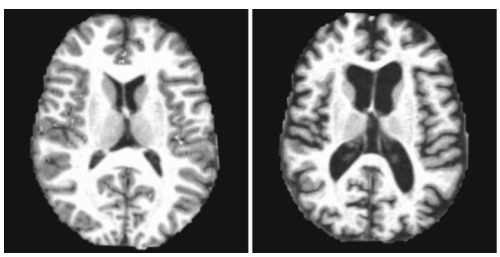

Fig. 1 Slice examples between (**a**) a nonalcoholic brain, and (**b**) an alcoholic brain

Materials

Subjects

The applicants went through a medical history interview to guarantee they met the inclusion criteria. Qualifying applicants received the computerized diagnostic interview schedule version IV, which ascertains the presence or absence of major psychiatric disorders. Applicants were excluded if mandarin is not their first language, if they were left-handed, or if they had HIV, epilepsy, stroke; Wernick Korsakoff syndrome; bipolar; cirrhosis or liver failure, or

Table 2 Division of our acquired 235-image dataset

	Alcoholic	Non-Alcoholic	Total
Training	50	50	100
Test	64	71	135
Total	114	121	235

Table 3 Data augmentation of original training dataset

	Total	Alcoholic	Non-Alcoholic
Original Training Dataset	100	50	50
Image Rotation	3000	1500	1500
Gamma Correction	3000	1500	1500
Noise Injection	3000	1500	1500
Random Translation	4000	2000	2000
Training Dataset after DA	13,100	6550	6550

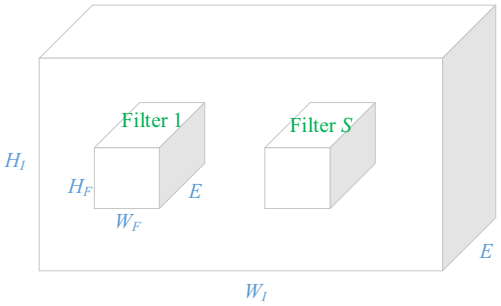

Fig. 3 Two-dimensional convolution operation

seizures unrelated to alcoholism, head injury with loss of consciousness more than 15 min unrelated to alcoholism, depression, schizophrenia, and other psychotic disorders.

Finally, we enrolled 114 abstinent long-term chronic alcoholic participants (58 men and 56 women) and 121 nonalcoholic control participants (59 men and 62 women). Participants were enrolled through flyers posted in Jiangsu Province Hospital, Nanjing Children's Hospital, and Nanjing Brain Hospital, as well as the internet-based advertisements. The subject enrollment and MRI scanning cost in total three years. The research was approved by the Institutional Review Board of the participating hospitals. In addition, informed consent was obtained from each participant.

The 235 participants were tested by the "Alcohol Use Disorder Identification Test (AUDIT)" [19]. The unit "ounce" was transformed to "gram", since the former is not widely identified in China (Table 1).

(DOHD = duration of heavy drinking; DDE = daily drinks of ethanol; AUDIT = alcohol use disorders identification test; LOS = length of sobriety).

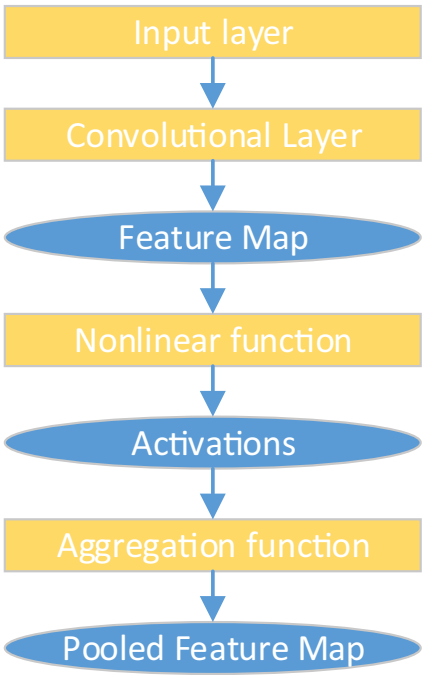

Fig. 2 Typical block in a CNN

Scan protocol

All 235 subjects lie as still as possible, with their eyes closed and keep conscious. Scanning was implemented by a Siemens Verio Tim 3.0 T MR scanner (Siemens Medical Solutions, Erlangen, Germany). In total 216 sagittal slices covering the whole brain were acquired, using an MP-RAGE sequence. The imaging parameters were listed as: TE = 2.50 ms, TR = 2000 ms, TI = 900 ms, FA = 9°, FOV = 256 mm × 256 mm, matrix = 256 × 256, slice thickness = 0.8 mm.

Slice selection

We used FMRIB software library (FSL) v5.0 software to extract brain and remove skulls for each scanned 3D image. All the volumetric images were normalized to a standard MNI template, which is the standard template in FSL software. Afterwards, we resampled each image to 2 mm isotropic voxel. The slice at $Z = 80$ voxels (8 mm) at MRI_152 coordinate was chosen for each patient. Background was cropped, leaving a rectangle matrix with size of 176 × 176, because of the ease for following classifier training. Two samples are shown in Fig. 1. The data are available upon request.

Table 4 Size of input, filter, and output

Operator	Size
Input	$H_I \times W_I \times E$
Filter	$H_F \times W_F \times E \times S$
Output	$H_O \times W_O \times S$

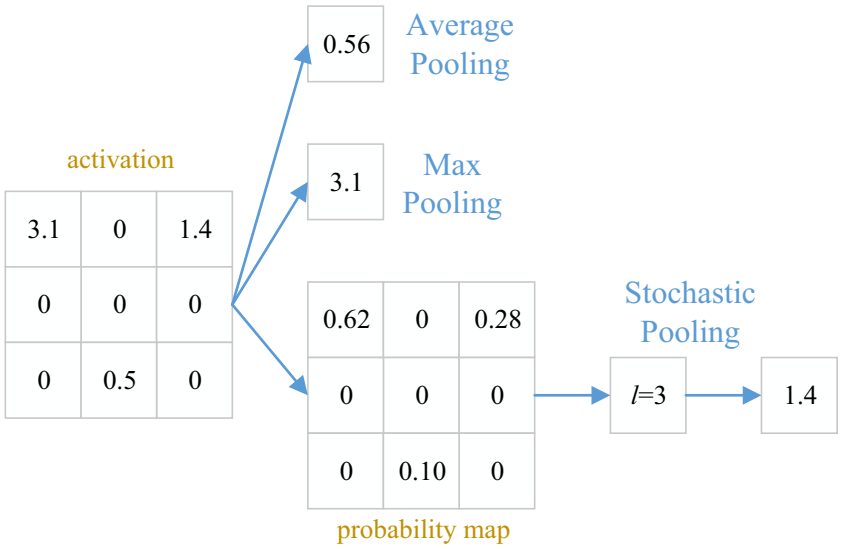

Fig. 4 A toy example using three different pooling techniques (*l* means a potential location selected randomly)

Data augmentation

The 235-image dataset is too small, since it is rather hard to enroll qualified patients. Deep learning usually requires a large dataset for learning a hierarchical representation, without overfitting to the training data [20]. Hence, data augmentation (DA) method is often used over the training data segmented from original data. The first data augmentation method is image rotation. The rotation angle θ is from $-15°$ to $15°$ in step of $1°$. Thus, we create 30 new samples. The second DA method is gamma correction.

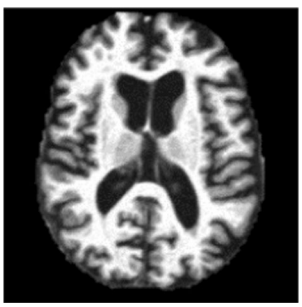

Fig. 5 An alcoholic image in the training set to be augmented

The gamma-value r varies from 0.7 to 1.3 with step of 0.02, again leading to 30 new samples. The third DA method is noise injection. We create 30 new noise-contaminated image for each image. The zero-mean Gaussian noise with variance of 0.01 was employed. The fourth DA method used random translation, and generated 40 new images.

The 235-image was split randomly into training set and test set as shown in Table 2. The training set contains 100-image with 50 alcoholic image and 50 non-alcoholic image. The test contains 135 images, containing 64 alcoholic image and 71 non-alcoholic image.

In this way, the training dataset after DA contains 13,100 image as shown in Table 3. Among it, 6550 are alcoholic brain slices, and the rest 6550 are non-alcoholic brain slices.

Convolutional neural network

Convolutional neural network (CNN) consists of alternating layers of convolution and pooling. The convolutional layer convolves a filter over the input layer, and output a feature

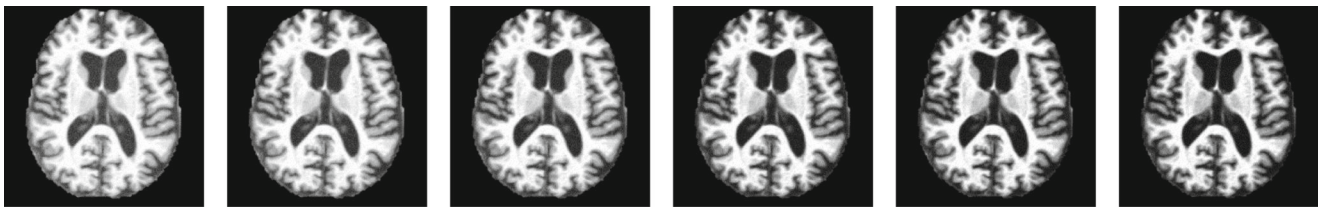

(a) 0.7 (b) 0.8 (c) 0.9 (d) 1.1 (e) 1.2 (f) 1.3

Fig. 6 Data augmentation by Gamma correction

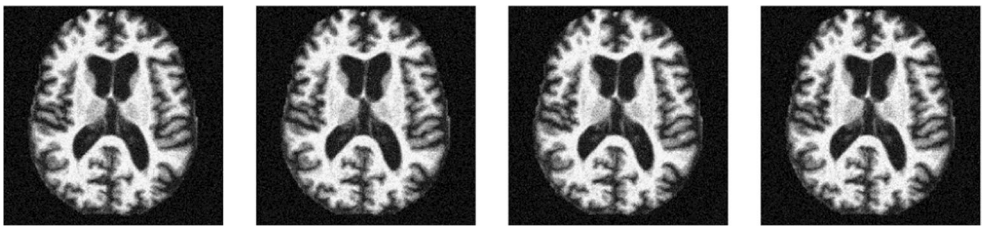

Fig. 7 Data augmentation by noise injection

map. A non-linear function is then applied element-wise to voxels within the feature map, and the resulting is called "activation". The activations are then passed to an aggregation function in the pooling layer, generating a pooled feature map as output. The above procedure is shown in Fig. 2. CNN has been proven to give better results than traditional classifiers, such as support vector machine, linear regression classifier [21, 22], etc.

Convolutional and rectified linear unit layer

In CNN, the convolution layer implements a 2D convolution for 3D input and 3D filter, since the channels of both input and filter are the same. Assume the size of the S filter is $H_F \times W_F \times E$, here H_F and W_F represent the height and width of the filters, E the channels. Assume the size of the input is $H_I \times W_I \times E$, here H_I represents the height, W_I the width. The 2D convolution is performed along the width and height directions (Fig. 3).

Suppose the stride size is T, the padding size at each margin is M. The height H_O and width W_O can be obtained as

$$H_O = 1 + \frac{H_I - H_F + 2M}{T} \tag{1}$$

$$W_O = 1 + \frac{W_I - W_F + 2M}{T} \tag{2}$$

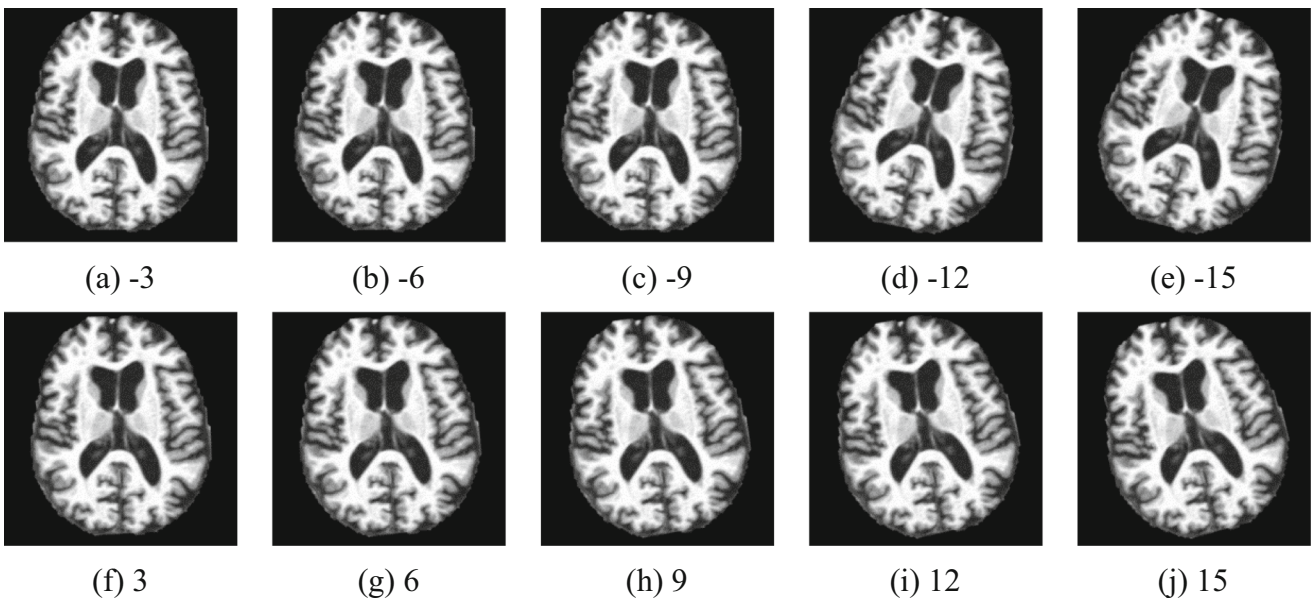

Fig. 8 Data augmentation by image rotation

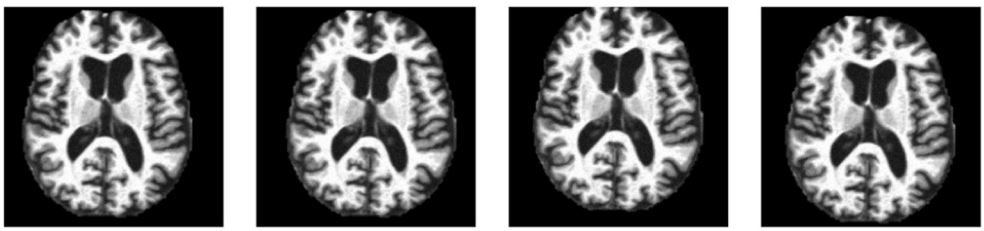

Fig. 9 Data augmentation by random translation

Table 5 Parameters of each layer in proposed CNN

Layer	Parameters
Conv_relu_1	Filter Size = 5 × 5; No of Filters = 40; Stride = 3 × 3
Conv_relu_2	Filter Size = 3 × 3; No of Filters = 80; Stride = 5 × 5
Pool_1	Pool size = 3 × 3; Stride = 1 × 1; Padding = 1 × 1
Conv_relu_3	Filter Size = 3 × 3; No of filters = 120; Stride = 1 × 1; Padding = 1 × 1
Pool_2	Pool size = 3 × 3; Stride = 1 × 1; Padding = 1 × 1
Conv_relu_4	Filter Size = 3 × 3; No of filters = 120; Stride = 1 × 1; Padding = 1 × 1
Pool_3	Pool size = 3 × 3; Stride = 1 × 1; Padding = 1 × 1
Conv_relu_5	Filter Size = 3 × 3; No of filters = 120; Stride = 1 × 1; Padding = 1 × 1
Pool_4	Pool size = 3 × 3; Stride = 3 × 3
Fully_connected_1	Weights = 50 × 1920; Bias = 50 × 1
Fully_connected_2	Weights = 2 × 50; Bias = 2 × 1

The output is 3D with size of $H_O \times W_O \times S$, where S denotes the number of filters defined before. W_I, W_F, and W_O represent width of input, filter, and output, respectively. The size of input, filter, and output are listed in Table 4.

The neurons in the feature map after convolution layer will pass through a nonlinear activation function, such as a rectified linear unit (ReLU) layer [23], which carries out a ReLU function as

$$ReLU(t) = \begin{cases} t & t \geq 0 \\ 0 & t < 0 \end{cases} \quad (3)$$

Pooling layer

The pooling layer modifies the outputs from the ReLU layer with a summary statistic of nearby outputs in a neighbored window. It has three advantages: (i) help the representation keep invariant to slight translation of the input; (ii) reduce the computation resources needed; (iii) help the activations in pooled map are less sensitive to the precise locations of structures than unpooled map.

Assume the pooling region is D, the activation set B included in D is

$$B = \{b_i | i \in D\} \quad (4)$$

The max-pooling P_M [24] is the most popular pooling strategy, with definition as

$$P_M = \max(B_D) \quad (5)$$

Average-pooling P_A [25] is defined as

$$P_A = \frac{\sum B_D}{|B_D|} \quad (6)$$

here |.| is the number of the elements in the set.

Stochastic-pooling (SP) [26] P_S selects the pooled map response by sampling from a multinomial distribution formed from the activations of each pooling region. Mathematically, the probability map p_i is first calculated based on original activation map b_i as

$$p_i = \frac{b_i}{\sum_B b_i} \quad (7)$$

Then, the output is sampled from the multinomial distribution to pick a location l within the activation region B as

$$P_S = b_l, where\ l \sim P(p_1, \ldots, p_i, \ldots) \quad (8)$$

Table 6 Hardware configuration of CNN

Parameter	Value
Compute capability	6.1
Clock rate	1455 MHz
Multiprocessors	5
Warp size	32
Registers per block	65,536
Threads per block	1024

Table 7 Algorithm setting of CNN Training

Parameter	Value
minibatch size	256
Initial learning rate	0.01
Drop period	10
Drop rate factor	0.1
Momentum	0.9
Maximum epoch	30
LF	cross entropy

Fig. 10 Training accuracy

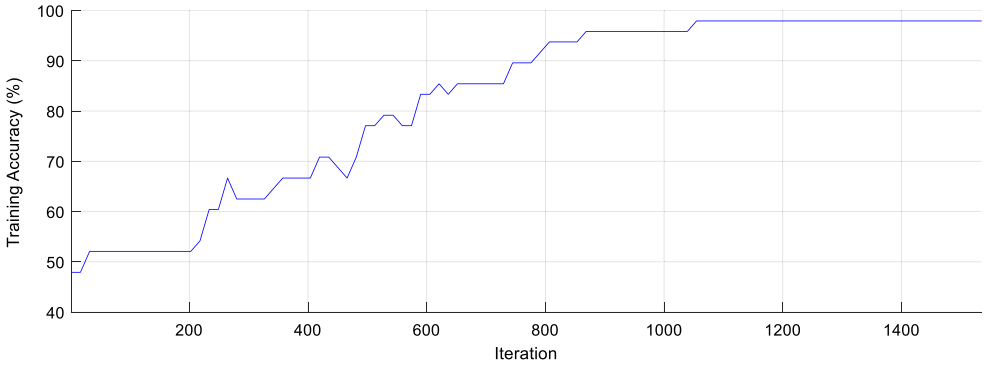

Fig. 11 Training loss

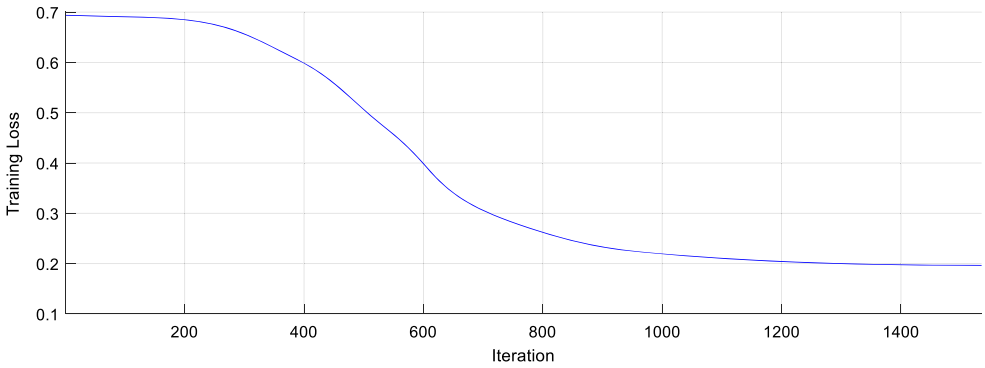

An example of above three polling techniques is shown in Fig. 4. Here the activation region is a 3 × 3 matrix. The average pooling and max pooling produces 0.56 and 3.1, respectively. For stochastic pooling, the probability map is first generated with $p_1 = 0.62$, $p_3 = 0.28$, and $p_8 = 0.10$. The multinomial distribution lets $l = 3$, and finally the output is 1.4. Note that there are other pooling techniques, such as hierarchical rank pooling [27], pyramid pooling [28], etc. In the future, our team shall check their performances.

Fully connected and softmax layer

The fully connected layer (FCL) multiplies the input to it by a weight matrix, and the multiplication result is added to a bias vector. The following softmax layer used the softmax function, i.e., the multiclass generalization of logistic regression [29]. The probability of sample x belonging to class c is defined as:

$$Y(c|x) = \frac{Y(x|c) \times Y(c)}{\sum_{k=1}^{C} Y(x|k) \times Y(k)} \tag{9}$$

Here $Y(x|c)$ is the conditional probability of sample given class c. $Y(c)$ is the class prior probability. C is the in-all number of classes. For simplicity, define Z_c as

$$Z_c = \ln(Y(x, c) \times Y(c)) \tag{10}$$

Finally, we have

$$Y(c|x) = \frac{\exp(Z_c(x))}{\sum_{k=1}^{C} \exp(Z_k(x))} \tag{11}$$

Table 8 Confusion matrix over test set

	Alcoholic	Non-alcoholic
Alcoholic	62	2
Non-alcoholic	2	69

Table 9 Comparison to state-of-the-art methods over our test set (Unit: %)

Method	Confusion Matrix	Sensitivity	Specificity	Accuracy
FA + PNN [11]	[56 8 1061]	87.50	85.92	86.67
IPSO [12]	[57 7 665]	89.06	91.55	90.37
HMI + SVM [14]	[58 6 863]	90.63	88.73	89.63
CNN + SP (Our)	[62 2 269]	96.88	97.18	97.04

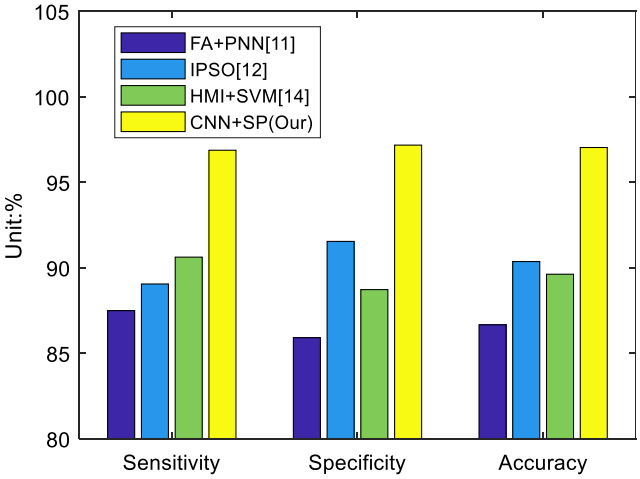

Fig. 12 Plot of our method compared to three state-of-the-art methods

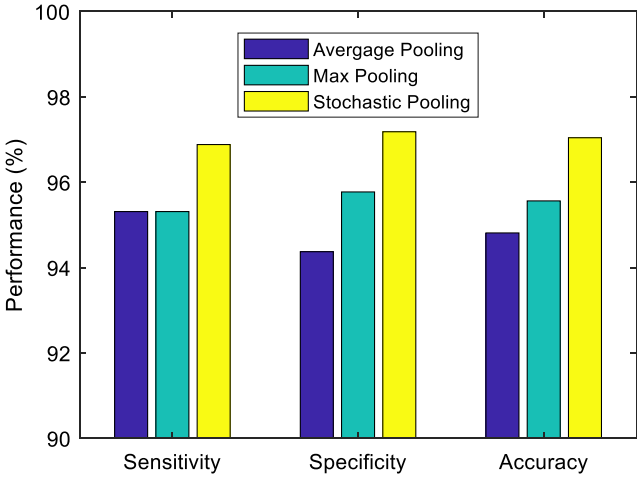

Fig. 13 Pooling comparison in terms of sensitivity, specificity, and accuracy over test set

Experiments and results

Data augmentation

Figure 5 shows an original alcoholic brain image. Figure 6 shows the data augmentation results by Gamma correction with typical values of 0.7, 0.8, 0.9, 1.1, 1.2, and 1.3, respectively. Figure 7 shows four samples of noise injection results. Figure 8 shows 10 data augmentation results by rotation. Finally, Fig. 9 shows four examples of random translation.

CNN structure

The structure of our CNN is adjusted by experience. The image input layer is with size of 176 × 176. Then, the setting of each following layer are listed in Table 5. Here we combine the convolutional layer and rectified linear unit layer as one layer. Finally, we append softmax layer and class output layer after the second fully connected layer.

CNN training

The CNN Training over the 13,100-image dataset was based on NVIDIA GeForce GTX 1050 with compute capability of 6.1, clock rate of 1455 MHz, and multiprocessors of 5. Table 6 shows the hardware configuration of CNN training.

Table 10 Pooling comparison

Pooling technique	Sensitivity	Specificity	Accuracy
Average pooling	95.31%	94.37%	94.81%
Max pooling	95.31%	95.77%	95.56%
Stochastic pooling	96.88%	97.18%	97.04%

The training algorithm was stochastic gradient descent with momentum (SGDM). The size of minibatch is set to 256. The initial learning rate is set to 0.01, and was decreased by factor of 10 every 10 epochs. The momentum was set to 0.9. The maximum epochs was assigned with a value of 30. Cross entropy [30] was used as the loss function (LF). Table 7 lists the algorithms setting of CNN training.

The training accuracy and training loss over 1535 iterations are shown in Fig. 10 and Fig. 11, respectively. We can observe that the accuracy increase gradually, and converge to 97.9167%. The loss decreases and converges to final 0.1965. Note the 1535 iterations correspond to 30 epochs in this study.

Performance over test set

The 135-image test set contains 64 alcoholic brain image and 71 non-alcoholic brain image. We used above CNN structure and chose stochastic pooling. The confusion matrix is listed in Table 8. Here the row corresponds to the actual class, and the column corresponds to the predicted class. For the 64 alcoholic brain images, 62 were correctly identified and 2 were misclassified as non-alcoholic brains. For the 71 non-

Table 11 Performance on different numbers of convolution layers

Number of convolution layers	Accuracy
2	82.96%
3	94.81%
4	95.56%
5 (Proposed)	97.04%
6	92.59%
7	96.30%

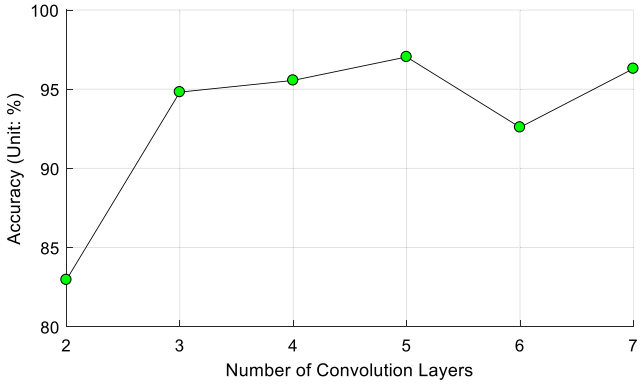

Fig. 14 Optimal structure—Effect of convolution layers

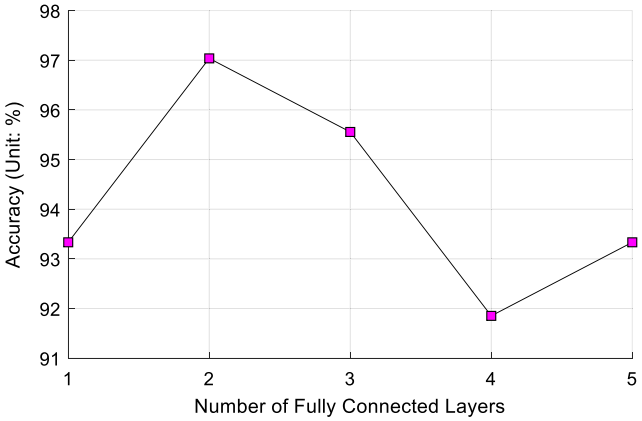

Fig. 15 Optimal structure—Effect of fully connected layers

alcoholic brain images, 69 were correctly identified and 2 were misclassified as alcoholic brains. Finally, the sensitivity is 96.88%, the specificity is 97.18%, and the accuracy is 97.04%.

Comparison to state-of-the-art approach

We compared this proposed method "CNN + SP" with three state-of-the-art approaches: FA + PNN [11], IPSO method [12], and HMI + SVM [14]. The results are shown in Table 9 and Fig. 12. The FA + PNN [11] obtained a sensitivity of 87.50%, a specificity of 85.92%, and an accuracy of 86.67%. The IPSO [12] obtained a sensitivity of 89.06%, a specificity of 91.55%, and an accuracy of 90.37%. HMI + SVM [14] obtained a sensitivity of 90.63%, a specificity of 88.73%, and an accuracy of 89.63%.

Nevertheless, our method significantly improves the classification performance, leading to a sensitivity of 96.88%, a specificity of 97.18%, and an accuracy of 97.04%. This suggests the powerfulness of convolutional neural network, which has already gained remarkable success in many other fields.

Pooling comparison

We compared the stochastic pooling with max pooling and average pooling. Their results were offered in Table 10. The graphical view is shown in Fig. 13.

Table 12 Performance on different numbers of fully connected layers

Number of fully connected layers	Accuracy
1	93.33%
2 (Proposed)	97.04%
3	95.56%
4	91.85%
5	93.33%

We observe that the stochastic pooling achieved the best performance among all thee pooling techniques. The average pooling has a drawback, that all elements in the pooling region are considered, thus it may down-weight strong activation due to many near-zero elements. The max pooling solves this problem, but it easily overfits the training set. Hence, max pooling does not generalize well to test set. The stochastic pooling [26] solve above two problems to some degree, and it gives superior performance to both average pooling and max pooling.

Optimal structure

The convolution layers are the most essential among all layers within CNN. Our CNN contains five convolution layers. Now we vary the number of convolution layers, and test the change of classification performance with the same settings in previous experiments. The comparison results were presented in Table 11 and Fig. 14.

As shown above, the accuracy results of CNNs varied with different convolution layers. The CNN with 2 convolution layers only achieved an accuracy of 82.96%, indicating that CNN with not well-tuned structure may give worse results than traditional classifiers [11, 12, 14]. From Fig. 14 we knew that the CNN with five convolution layers performs the best, which is the case as described in CNN structure section.

Table 13 Time Analysis

Training (per image)	Time (second)
CPU	17.35
GPU	0.1164
Acceleration	149
Test (per image)	Time (second)
CPU	3.149×10^{-2}
GPU	1.898×10^{-4}
Acceleration	166

Next, we check why two fully connect layers are the best. We vary the number from 1 to 5, and the results are listed in Table 12 and Fig. 15. Similarly, we can observe that the optimal number of fully connected layers is 2 in this study of alcoholism detection.

CPU versus GPU

In the final experiment, we compare the GPU with CPU in terms of computation time. The CPU is Intel Core i5–3470 with frequency of 3.20GHz. The computation time per image over training and test set are provided in Table 13, where four significant figures are reserved. We can observe that the GPU yielded a 149× acceleration in training and a 166× acceleration in test.

Conclusion

In this study, our team developed a novel alcoholism detection method, which is based on the hottest tool—convolutional neural network. This study compares three pooling techniques: max pooling, average pooling, and stochastic pooling. The results show the superiority performance of stochastic pooling. Besides, our proposed method outperforms three state-of-the-art approaches. We validated CNN with five convolution layers and two fully connected layers performed the best. GPU yielded a 149× acceleration in training and a 166× acceleration in test.

In the future, we shall try advanced variants of CNN. We shall also test different activation functions, such as leaky ReLU. Our method can be combined to communication systems [31, 32] and internet of things.

Acknowledgments This paper is financially supported by Natural Science Foundation of China (61602250) and Natural Science Foundation of Jiangsu Province (BK20150983).

Compliance with Ethical Standards

Conflict of Interest The authors declare there is no conflict of interest with regards to this submission.

References

1. Edwards, A.C., Lonn, S.L., Karriker-Jaffe, K.J., Sundquist, J., Kendler, K.S., and Sundquist, K., Time-specific and cumulative effects of exposure to parental externalizing behavior on risk for young adult alcohol use disorder. *Addict. Behav.* 72:8–13, 2017. https://doi.org/10.1016/j.addbeh.2017.03.002.
2. Wlodarczyk, O., Schwarze, M., Rumpf, H.J., Metzner, F., and Pawils, S., Protective mental health factors in children of parents with alcohol and drug use disorders: A systematic review. *PLoS One*. 12(6):15, 2017. Article ID e0179140. https://doi.org/10.1371/journal.pone.0179140.
3. Kobayashi, T., Monma, M., Baba, T., Ishimori, Y., Shiotani, S., Saitou, H., Kaga, K., Miyamoto, K., Hayakawa, H., and Homma, K., Optimization of inversion time for postmortem short-tau inversion recovery (STIR) MR imaging. *Magn. Reson. Med. Sci.* 13(2): 67–72, 2014. https://doi.org/10.2463/mrms.2013-0046.
4. Murano, T., Koshimizu, H., Hagihara, H., and Miyakawa, T., Transcriptomic immaturity of the hippocampus and prefrontal cortex in patients with alcoholism. *Sci. Rep.* 7(8), 2017. Article ID 44531. https://doi.org/10.1038/srep44531.
5. Sawyer, K.S., Oscar-Berman, M., Ruiz, S.M., Galvez, D.A., Makris, N., Harris, G.J., and Valera, E.M., Associations between cerebellar subregional morphometry and alcoholism history in men and women. *Alcoholism*. 40(6):1262–1272, 2016. https://doi.org/10.1111/acer.13074.
6. Liao, X., Yin, J., Guo, S., Li, X., and Sangaiah, A.K., Medical JPEG image steganography based on preserving inter-block dependencies. *Comput. Electr. Eng.* https://doi.org/10.1016/j.compeleceng.2017.08.020.
7. Zhang, R., Shen, J., Wei, F., Li, X., and Sangaiah, A.K., Medical image classification based on multi-scale non-negative sparse coding. *Artif. Intell. Med.*, 2017. https://doi.org/10.1016/j.artmed.2017.05.006.
8. Samuel, O.W., Zhou, H., Li, X., Wang, H., Zhang, H., Sangaiah, A.K., and Li, G., Pattern recognition of electromyography signals based on novel time domain features for amputees' limb motion classificationPattern recognition of electromyography signals based on novel time domain features for amputees' limb motion classification. *Comput. Electr. Eng.* 2017. https://doi.org/10.1016/j.compeleceng.2017.04.003.
9. Fisher, T., Hamed, A., Vartholomeos, P., Masamune, K., Tang, G.Y., Ren, H.L., and Tse, Z.T.H., Intraoperative magnetic resonance imaging-conditional robotic devices for therapy and diagnosis. *Proc. Inst. Mech. Eng. Part H. J. Eng. Med.* 228(3):303–318, 2014. https://doi.org/10.1177/0954411914524189.
10. Nayak, D.R., Dash, R., and Majhi, B., Brain MR image classification using two-dimensional discrete wavelet transform and AdaBoost with random forests. *Neurocomputing*. 177:188–197, 2016. https://doi.org/10.1016/j.neucom.2015.11.034.
11. Alweshah, M., and Abdullah, S., Hybridizing firefly algorithms with a probabilistic neural network for solving classification problems. *Appl Soft Comput*. 35:513–524, 2015. https://doi.org/10.1016/j.asoc.2015.06.018.
12. Lv, Y.-D., and Hou, X.-X., Alcoholism detection by medical robots based on Hu moment invariants and predator–prey adaptive-inertia chaotic particle swarm optimization. *Comput. Electr. Eng.* https://doi.org/10.1016/j.compeleceng.2017.04.009.
13. Monnig, M.A., Observed power and projected sample sizes to detect white matter atrophy in neuroimaging of alcohol use disorders. *Alcoholism*. 36:272A–272A, 2012.
14. Yang, J., Pathological brain detection in MRI scanning via Hu moment invariants and machine learning. *J. Exp. Theor. Artif. Intell.* 29(2):299–312, 2017. https://doi.org/10.1080/0952813X.2015.1132274.
15. Do, B.J., Park, I.Y., Rhee, S.Y., Song, J.K., Jang, M.K., Cho, S.J., Nam, E.S., and Yun, E.J., A case of multiple hypervascular hyperplastic liver nodules in a patient with no history of alcohol abuse or chronic liver diseases. *Korean J. Gastroenterol.* 65(5):321–325, 2015. https://doi.org/10.4166/kjg.2015.65.5.321.
16. Matsui, T., Sakurai, H., Toyama, T., Yoshimura, A., Matsushita, S., and Higuchi, S., Clinical application of neuroimaging to alcohol-related dementia. *Jpn. J. Alcohol Stud. Drug Depend.* 47(3):125–134, 2012.
17. Zahr, N.M., Kaufman, K.L., and Harper, C.G., Clinical and pathological features of alcohol-related brain damage. *Nat. Rev. Neurol.* 7(5):284–294, 2011. https://doi.org/10.1038/nrneurol.2011.42.

18. Bae, J., Cha, Y.J., Lee, H., Lee, B., Baek, S., Choi, S., and Jang, D., Social networks and inference about unknown events: A case of the match between Google's AlphaGo and Sedol Lee. *PLoS One*. 12(2):25, 2017. Article ID e0171472. https://doi.org/10.1371/journal.pone.0171472.
19. Barik, A., Rai, R.K., and Chowdhury, A., Alcohol use-related problems among a rural Indian population of West Bengal: An application of the alcohol use disorders identification test (AUDIT). *Alcohol Alcohol*. 51(2):215–223, 2016. https://doi.org/10.1093/alcalc/agv097.
20. Lakhani, P., Deep convolutional neural networks for endotracheal tube position and X-ray image classification: Challenges and opportunities. *J. Digit. Imaging*. 30(4):460–468, 2017. https://doi.org/10.1007/s10278-017-9980-7.
21. Chen, Y., and Jin, Z., Reconstructive discriminant analysis: A feature extraction method induced from linear regression classification. *Neurocomputing*. 87:41–50, 2012. https://doi.org/10.1016/j.neucom.2012.02.001.
22. Chen, Y., Li, Z.Z., and Jin, Z., Feature extraction based on maximum nearest subspace margin criterion. *Neural. Process. Lett.* 37(3):355–375, 2013. https://doi.org/10.1007/s11063-012-9252-y.
23. Barushka, A., and Hajek, P., Spam filtering using regularized neural networks with rectified linear units. In: Adorni, G., Cagnoni, S., Gori, M., Maratea, M., (Eds.), *15th International Conference of the Italian Association for Artificial Intelligence (AIIA), Genova, ITALY. Lecture Notes in Computer Science*. Springer Int Publishing Ag, 2016, pp 65–75. https://doi.org/10.1007/978-3-319-49130-1_6.
24. Sun, M., Raju, A., Tucker, G., Panchapagesan, S., Fu, G. S., Mandal, A., Matsoukas, S., Strom, N., and Vitaladevuni, S., Max-pooling loss training of long short-term memory networks for small-footprint keyword spotting. In: *IEEE workshop on spoken language technology* (SLT), San Diego, CA, USA: IEEE, 2016, pp 474–480.
25. Zhu, S.G., and Du, J.P., Visual tracking using max-average pooling and weight-selection strategy. *J. Appl. Math.* Article ID 828907, 2014. https://doi.org/10.1155/2014/828907.
26. Zeiler, M. D., and Fergus, R., Stochastic pooling for regularization of deep convolutional neural networks, in: International Conference on Learning Representations (ICLR), Scottsdale, Arizona, USA,: IEEE, May 2, 2013, pp 1–7.
27. Fernando, B., and Gould, S., Discriminatively learned hierarchical rank pooling networks. *Int. J. Comput. Vis.* 124(3):335–355, 2017. https://doi.org/10.1007/s11263-017-1030-x.
28. Han, X.B., Zhong, Y.F., Cao, L.Q., and Zhang, L.P., Pre-Trained AlexNet Architecture with Pyramid Pooling and Supervision for High Spatial Resolution Remote Sensing Image Scene Classification. *Remote Sens*. 9(8):22, 2017. Article ID 848. https://doi.org/10.3390/rs9080848.
29. Zhan, T.M., and Chen, Y., Multiple sclerosis detection based on biorthogonal wavelet transform, RBF kernel principal component analysis, and logistic regression. *IEEE Access*. 4:7567–7576, 2016. https://doi.org/10.1109/ACCESS.2016.2620996.
30. Sahin, R., Cross-entropy measure on interval neutrosophic sets and its applications in multicriteria decision making. *Neural Comput. Appl.* 28(5):1177–1187, 2017. https://doi.org/10.1007/s00521-015-2131-5.
31. Chen, X.Q., and Wu, L.A., Nonlinear demodulation and channel coding in EBPSK scheme. *Sci. World J.* Article ID 180469, 2012. https://doi.org/10.1100/2012/180469.
32. Chen, X.Q., and Wu, L.N., A novel detection scheme for EBPSK system. *Math Probl. Eng.* Article ID 956191, 2012. https://doi.org/10.1155/2012/956191.